An evaluation of actinide reactivity with CO_2, O_2, and O_2/He gases using ICP-MS/MS: Application to simultaneous measurement of $^{241}Am/^{241}Pu$ ratios in unseparated complex matrices

Authors: Tyler D. Schlieder[1], *Kirby P. Hobbs[1], Amanda D. French[1]*, Lee H. Hughes[1], Isaac J. Arnquist[1], Chelsie Beck[1]*

[1]Pacific Northwest National Laboratory, Richland, WA, 99352 USA
*corresponding author; email: amanda.french@pnnl.gov

Abstract

Accurate actinide measurements are critical within the field of nuclear science. Traditional methods for actinide quantification require time-consuming sample processing prior to analysis. There is a need for rapid analytical techniques that still maintain a high degree of accuracy. In this work, actinide reactivity was assessed for multiple oxygen-containing reaction gases using quadrupole inductively coupled plasma tandem mass spectrometry (Q-ICP-MS/MS) to evaluate actinide analysis in complex sample matrices without analyte-matrix separation. A novel method was developed to measure $^{241}Am/^{241}Pu$ in complex sample matrices using O_2/He reaction gas with no matrix removal or analyte pre-concentration. This inline method reduces matrix-derived polyatomic interferences that complicate traditional ICP-MS analyses by mass-shifting to $^{241}Am^{16}O^+$ and $^{241}Pu^{16}O_2^+$, allowing Am and Pu to be mass separated for simultaneous analysis. While mass shifting is efficient, a small portion of Am^+ (<1.3%) and Pu^+ (<1.4%) react to form AmO_2^+ and PuO^+, respectively. Therefore, a mass balance approach was used, in combination with reactivity determined from ^{242}Pu and ^{243}Am standard solutions, to correct for residual $^{241}PuO^+$ and $^{241}AmO_2^+$. The method was validated by measuring $^{241}Am/^{241}Pu$ in Pu isotope standards CRM-136 and CRM-137 (separated in March/April 1970 and February 2022, respectively) in both neat solutions and complex matrices containing diluted soil (NIST SRM 2711a, >1000 $\mu g \cdot g^{-1}$). Method detection limits of 15.9 $fg \cdot g^{-1}$ and 9.6 $fg \cdot g^{-1}$ were determined for ^{241}Am and ^{241}Pu, respectively, and $^{241}Am/^{241}Pu$ ratios were measured with accuracies within <3.5%. This work presents the first direct analysis of $^{241}Am/^{241}Pu$ in unseparated complex matrices, advancing capabilities for rapid actinide measurements.

The rapid and accurate determination of actinide concentrations and isotopic ratios is critical for many aspects of nuclear science, including management of radioactive waste produced in the nuclear industry, [1] characterization of nuclear debris for decommissioning, [2-4] environmental monitoring, [5-8] and nuclear forensics. [9-11] Numerous analytical techniques have been developed for measuring actinides, with the two most common approaches being radiometric and mass spectrometric (MS) methods. While radiometric methods, such as α-spectrometry, β-counting, and γ-spectroscopy, are well suited for actinides with a high specific activity (i.e., short half lives), they are generally less sensitive for longer lived (>100 years) radioisotopes (e.g., ^{237}Np). [12, 13] Additionally, sample throughput using radiometric methods is often limited by long counting times, and substantial sample processing required to isolate target analytes from matrix and interference isotopes (e.g., ^{228}Th from ^{241}Am). [12, 13] Mass spectrometric techniques, while more expensive than radiometric analysis, are often considered analytically superior for actinide measurements due to shorter analysis times, smaller sample sizes, multi-element

capabilities, and improved analytical precision. The most widely applied MS techniques for making actinide measurements include thermal ionization mass spetrometry (TIMS) and inductively coupled plasma mass spectrometry (ICP-MS).

Thermal ionization mass spectrometry has been widely considered the gold standard for determining isotopic ratios and concentrations for the actinides [14]. This can be attributed to the highly accurate and precise (<0.1% or sub-per mil) isotopic ratios achievable when used with a multi-collector (MC) array. A complicating factor of TIMS analysis is that it requires a chemically pure analyte because of the suppressive effect of impurities on ion formation. [14] Multi-collector (MC)-ICP-MS, an alternative to TIMS, has garnered increased attention for actinide analysis as its interface allows for a greater degree of versatility while still achieving similar levels of accuracy and precision. [15-18] However, as with TIMS, MC-ICP-MS methods for actinide measurements still require chemical purification, in this case to overcome isobaric and polyatomic interferences derived from matrix elements (e.g., $^{239}Pu^{+}$-$^{238}U^{1}H^{+}$, $^{238}Pu^{+}$-$^{238}U^{+}$,$^{239}Pu^{+}$-$^{207}Pb^{16}O_2^{+}$,$^{241}Pu^{+}$-$^{241}Am^{+}$, etc.). [19-23] An alternative approach for interference removal uses quadrupole tandem ICP-MS (Q-ICP-MS/MS) which can efficiently remove matrix- and plasma-derived polyatomic and isobaric interferences through the use of a collision/reaction gas. Quadrupole-ICP-MS/MS uses a collision reaction cell (CRC) that contains a multipole (quadrupole, hexapole, or octopole) which is set between two quadrupole mass analyzers capable of mass filtering at 1 amu based on the mass/charge (*m/z*) ratio of ions. Using this configuration, all ions with the same *m/z* are introduced into the CRC where they can be separated based on differences in gas-phase ion-molecule reactivity, allowing for inline separations, and significantly reducing (or even eliminating) the need for time-consuming chemical separations prior to analysis.

A number of recent publications have investigated the utility of Q-ICP-MS/MS techniques for making actinide measurements. These studies range from fundamental investigations evaluating Np^{+}, Am^{+}, and Cm^{+} reactivity with O_2 and CO_2 gas with the goal of improving ultra-trace analysis of nuclear fuel materials, [2] to targeted applications, such as investigating N_2O, CO_2, and O_2 gases for mitigating $^{235}U^{1}H^{+}$ interference on $^{236}U^{+}$ when measuring low $^{236}U/^{238}U$ ratios. [5, 6, 24] For the latter example, Q-ICP-MS/MS enabled the accurate determination of ultra-low $^{236}U/^{238}U$ (10^{-11}) for the first time using O_2 as the reaction gas. [6] While Q-ICP-MS/MS techniques continue to be developed for many of the actinides, perhaps the most widely targeted application has been for Pu isotope analysis. Accurately measuring Pu isotopes with ICP-MS is complicated by numerous matrix-derived interferences (e.g. $^{238}U^{+}$-$^{238}Pu^{+}$, $^{239}Pu^{+}$-$^{238}U^{1}H^{+}$, $^{207}Pb^{16}O_2^{+}$, $^{241}Am^{+}$-$^{241}Pu^{+}$, etc.), the most challenging to overcome being those associated with $^{238}U^{+}$ (i.e., $^{238}U^{+}$-$^{238}Pu^{+}$, $^{239}Pu^{+}$-$^{238}U^{1}H^{+}$, $^{240}Pu^{+}$-$^{238}U^{1}H_2^{+}$). Several reaction gases have been evaluated with

the intention of mitigating these interferences, including O_2, [21, 22, 25] CO_2, [21, 22, 25] NH_3, [1, 7, 19, 26-31] H_2, [29] and NO. [7, 11, 32] While all of these gases are effective for interference removal to some degree, several have proven particularly efficient. For example, CO_2 can reduce $^{238}UH^+$ interferences to $<1 \times 10^{-8}$ by mass shifting $^{238}U^+$ to $^{238}U^{16}O^+$ and leaving the majority of $^{239}Pu^+$ unreacted. [19] While this approach can significantly reduce interferences associated with $^{238}UH^+$, analyses of $^{239}Pu^+$ on mass are still susceptible to other matrix-derived interferences (e.g., $^{207}Pb^{16}O_2^+$). [19] Methods using NO gas can achieve similar levels of removal of direct atomic isobaric interferences (i.e., $^{238}U^+$) when targeting $^{238}Pu^+$, with the added benefit of mass shifting Pu^+ to $Pu^{16}O^+$, thus allowing for direct analysis of ultra-trace levels of ^{238}Pu in unseparated environmental sample matrices containing high levels of ^{238}U ($^{238}U/^{238}Pu = 8.2 \times 10^4$). [32] To date, the most efficient reported $^{238}UH^+$ interference removal for $^{239}Pu^+$ analysis has been achieved using NO gas ($^{238}UH^+$ interference mitigated to $<3.85 \times 10^{-11}$). [11, 32]

Another challenging actinide measurement that has benefited from ICP-MS/MS techniques is the analysis of ^{241}Am. Americium-241 accumulates in the environment due to ingrowth from ^{241}Pu fallout associated with nuclear weapons tests, nuclear accidents, and nuclear reprocessing plants. [33-35] Due to a relatively long half-life ($t_{1/2}$ = 432.7 yrs) ^{241}Am can stay in the environment for a significant amount of time and is useful for a number of applications including, nuclear forensics (i.e., age dating of Pu materials), sediment dating, oceanography and environmental radioactivity assessment. [33,4, 36-38] Similar to ^{239}Pu, direct measurement of $^{241}Am^+$ via ICP-MS is hindered by isobaric (i.e., $^{241}Pu^+$) and matrix-derived polyatomic interferences (e.g., $^{206}Pb^{35}Cl^+$, $^{208}Pb^{16}O_2{}^1H^+$, $^{201}Hg^{40}Ar^+$, $^{209}Bi^{32}S^+$, etc.); therefore, traditionally requiring chemical separation prior to analysis. [38-42] A particularly difficult challenge to overcome when measuring $^{241}Am^+$ is the isobaric interference from $^{241}Pu^+$, which would require a resolving power ($m/\Delta m$) of $>1 \times 10^7$ to resolve, exceeding the capabilities of commercially available instrumentation. As such, $^{241}Am^+$ reactivity has been evaluated with several gases (CO_2, [2, 7, 28] O_2, [2, 25, 39, 43, 44] NO, [7] C_2H_4, [7] and NH_3 [23]) to access efficiency of interference removal for ^{241}Am analysis by ICP-MS/MS, with particular focus on the removal of ^{241}Pu. Ethylene gas (C_2H_4), while effective for $^{238}U^+$-$^{238}Pu^+$ separation, does not appear to appreciably separate $^{241}Am^+$ and $^{241}Pu^+$. [7] Using He-NH_3 has been shown to reduce matrix-derived polyatomic interferences when measuring $^{241}Am^+$ on mass, but does not effectively separate $^{241}Am^+$ from $^{241}Pu^+$, and thus must be coupled with chemical separation to remove Pu. [23] Both CO_2 and NO shift $^{241}Pu^+$ to $^{241}Pu^{16}O^+$ and leave the majority of $^{241}Am^+$ on mass at m/z = 241 which effectively separates $^{241}Am^+$ and $^{241}Pu^+$; [2, 7, 11, 28] however, $^{241}Am^+$ on mass remains susceptible to matrix-derived polyatomic interferences. In contrast, O_2 gas predominantly mass shifts $^{241}Am^+$ to $^{241}Am^{16}O^+$ and $^{241}Pu^+$ to $^{241}Pu^{16}O_2^+$, [2, 25, 43-45] separating both $^{241}Am^+$ and $^{241}Pu^+$ from one another while also separating $^{241}Am^+$ from potential

polyatomic interferences at *m/z* = 241. Indeed, O_2 gas, in conjunction with chemical separation, has been successfully implemented for ultra-trace analysis (LOD = 0.17 $fg \cdot g^{-1}$) of ^{241}Am in soils. [45] However, in every previous Q-ICP-MS/MS method to date ^{241}Am analysis is coupled with some form of chemical separation prior to analysis, [23, 36, 39, 43, 45] which is often complex and time consuming. Furthermore, both ^{241}Am and ^{241}Pu are analytes of interest for some applications (e.g., dating of Pu materials), [37, 38] and currently all mass spectrometric methods require they be chemically separated from one another and analyzed individually. [36] There is a need for rapid and accurate ^{241}Am and ^{241}Pu analyses in complex sample matrices with less complicated and time-consuming sample preparation procedures.

In this work, gas-phase reactivity of the actinides (Pa, Th, Np, U, Pu, Am, Cm) with CO_2, O_2, and O_2/He reaction gas was investigated to evaluate potential gas-phase actinide separations by Q-ICP-MS/MS. These data were used to develop a Q-ICP-MS/MS method for inline ^{241}Am-^{241}Pu separation which allows for direct measurement of $^{241}Am/^{241}Pu$ ratios in complex sample matrices with no need for complex front-end chemistry. Examples of $^{241}Am/^{241}Pu$ analysis of two Pu isotopic standards with different separation dates (c.a. 1970 and 2022) are provided. The method was further verified for complex sample matrices by measuring $^{241}Am/^{241}Pu$ ratios in spiked standard reference material NIST SRM 2711a containing ~1095 $\mu g \cdot g^{-1}$ sample matrix. To the best of the authors knowledge this is the first work demonstrating direct analysis of $^{241}Am/^{241}Pu$ in unseparated complex sample matrices.

Methods

Reagents and materials

Standard solutions were prepared from stock standards of ^{nat}U (Inorganic Ventures; Christiansburg, VA), $^{239,242}Pu$ (NBL-CRM-128), ^{237}Np (Eckert & Ziegler Isotope Products; Valencia, CA), and ^{248}Cm (Oak Ridge National Laboratory, Oak Ridge, TN). Additionally, sources of ^{231}Pa and ^{243}Am were obtained from Eckert & Ziegler (Valencia, CA). Actinide reactivity experiments were conducted using standard solutions comprised of ^{231}Pa, ^{232}Th, ^{237}Np, ^{238}U, $^{239,242}Pu$, ^{243}Am, and ^{248}Cm. All standards were diluted with 2% HNO_3 (Optima grade; Fisher Scientific; Pittsburgh, PA) and ≥ 18.2 MΩ·cm deionized water. Helium (He; 99.999% purity; Oxarc), oxygen (O_2; 99.999% purity; Advanced Specialty Gases; Reno, NV), carbon dioxide (CO_2; 99.99%; Oxarc), and mixed O_2/He (9.88% O_2, remainder He, 99.999%, Oxarc; Spokane, WA) gases were used as collision/reaction gases and were further purified with an inline gas purifier (Entegris, Billerica, MA). Americium/Pu analysis methods were developed using ^{243}Am and ^{242}Pu solutions and refined using Pu isotope standards CRM-136 and CRM-137. NIST SRM 2711a (Montana soil) was used to produce complex matrix solutions. CRM-136 (previously SRM 946) underwent purification to remove Am between March-April 1970. [37] CRM-137 (previously SRM 947) was initially

produced September 1970, [37] and the aliquot measured here underwent purification from Am at Pacific Northwest National Laboratory on 2/2/2022.

Instrumentation

All analyses were conducted using an Agilent 8900 Q-ICP-MS/MS instrument (Agilent Technologies, Santa Clara, CA). The instrument is comprised of two quadrupole mass filters and an octopole ion guide contained within a CRC. The CRC is located between the quadrupole mass filters which are denoted as Q1 (located before the CRC) and Q2 (located after the CRC). Q1 mass resolves the ions before the CRC, where they interact with the collision/reaction gas. The octopole ion guide radially constrains the ions within the CRC, minimizing spread of the beam and ensuring efficient transmission of (product) ions into Q2. Product and unreacted ions are then mass resolved by Q2. The instrument has a maximum *m/z* range of 275 amu on Q2, which limits the detection of higher order products for the actinides. The instrument is equipped with a 250 $\mu L \cdot min^{-1}$ microflow PFA nebulizer (Elemental Scientific, Omaha, NE, USA), a Peltier cooled quartz double-pass spray chamber, s-lens, and Pt sampler and skimmer cones. General tuning parameters can be found in the Supporting Information (Table S1).

The sensitivity of the instrument was assessed with no gas in the CRC to determine the transmission efficiency at different gas flows in MS/MS mode. For this work, the O_2/He mix was analyzed using the 3rd cell line to increase the amount of O_2 being added to the CRC. When using the 3rd mass flow controller (MFC), a minimum of 1 $mL \cdot min^{-1}$ He must also be used; thus, the O_2/He mix was analyzed with additional He. Non-diluted O_2 and CO_2 were analyzed on the 4th cell line (Supporting Information). Actinide product distributions were measured at four flow rates (Supporting Information) to assess how product distribution changes with increasing flow (pressure) in the CRC. Selected flow rates span the range allowed by the MFC on each line. At each flow rate, the instrument sensitivity was optimized using the Deflect (focusing voltage applied after the octopole, prior to Q2), OctP Bias (used to control ion kinetic energy), and energy discrimination (the difference between the Q2 and octopole biases) parameters (see Table S3 for measured sensitivities). For these experiments Q1 was set to *m/z* = M^+ (reactant ion) and Q2 was set to mass scan from *m/z* of M^+ to 275.

Results and Discussion

General reactivity of actinide ions (Pa^+, Th^+, Np^+, U^+, Pu^+, Am^+, and Cm^+) with CO_2, O_2, and O_2/He

Measured reactivity of actinide ions (Pa^+, Th^+, Np^+, U^+, Pu^+, Am^+, and Cm^+) with CO_2, O_2, and O_2/He gases are shown in Fig. 1. A detailed discussion of reactivity of all measured actinides is provided

in the Supporting Information. For brevity, results presented herein focus on 1) reactivity of Am^+ and Pu^+ and 2) instances where newly acquired data deviate from previous literature. In general, the actinide ions react with CO_2 to form MO^+ and MO_2^+ species, although appreciable amounts of Am^+ remain

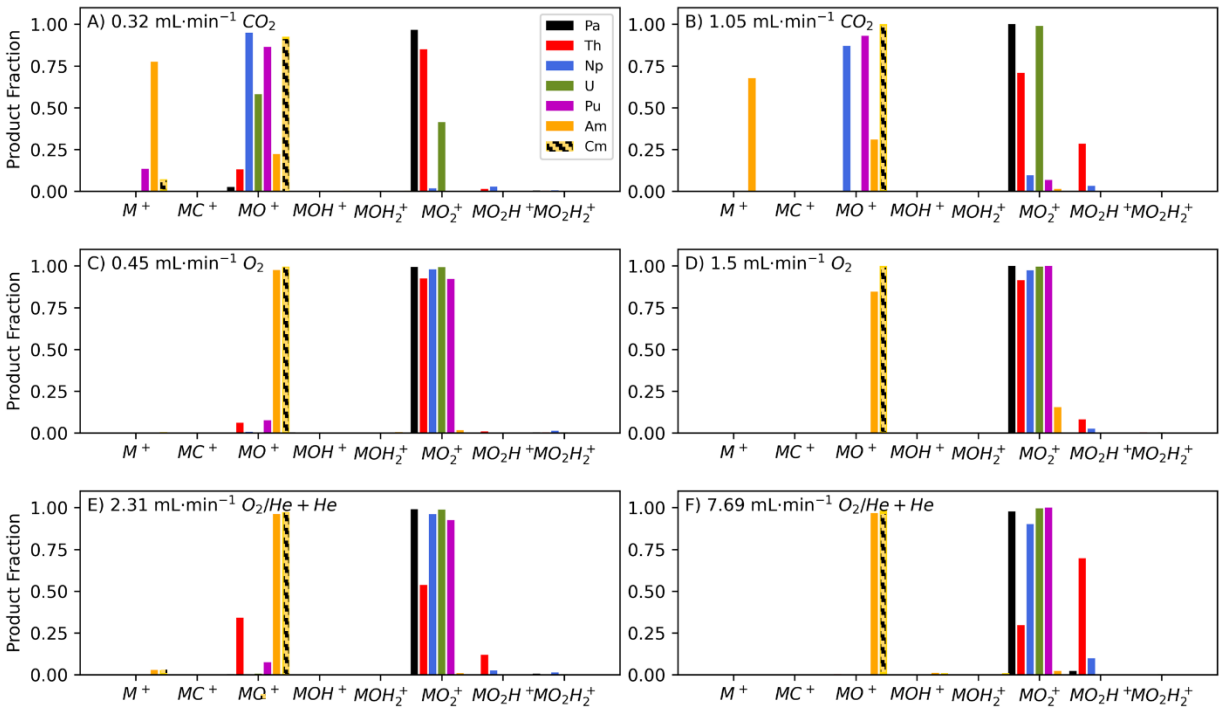

Figure 1: Actinide reactivity with CO_2 (A-B), O_2 (C-D), and O_2/He (E-F) gas. O_2/He + He data were collected using 8 mL·min^{-1} He at all flow rates of O_2/He mixed gas. Hatch marks denote Cm which has a MO_2^+ products where the *m/z* exceeds the maximum of the Agilent 8900 (*m/z* = 275).

unreacted (Fig. 1). Increasing CO_2 flow rate shifts formation to higher order oxide products, with both Pu^+ and Am^+ forming more MO^+ product. Plutonium$^+$ predominantly forms the MO^+ product; however, at low flow rates (0.16 mL·min^{-1}) ~50% of Pu^+ remains on mass (Fig. 1; Supporting Information). Americium was the least reactive actinide with CO_2, with >90% of Am^+ remaining on mass (at M^+) at low flow rates (Fig. 1; Supporting Information). Using higher CO_2 flow rates does facilitate the formation of AmO^+; however, at the maximum CO_2 flow rate (1.05 mL·min^{-1}) ~68% of Am^+ remains unreacted (Fig. 1). The trends in actinide reactivity with CO_2 reported here are similar to what has been observed for the lanthanides, [46] and in general, are consistent with actinide reactivites reported elsewhere [1, 2, 31]. The only exception is the observed behavior of U^+ at higher CO_2 flow rates. This work showed that at CO_2 flow rates ≥60% (≥0.63 mL·min^{-1}) U^+ predominantly forms MO_2^+ vs. MO^+, which is consistent with Cox et al. [28], but contrasts with other studies that find U^+ reacts to primarily form MO^+ even at high CO_2 flow rates (>0.5 mL·min^{-1}). [1, 29-31] The exact source of this discrepancy is difficult to ascertain, however, recent work [47]

demonstrating the importance of ion kinetic energy for interference removal when using Q-ICP-MS/MS observed that more UO_2^+ product was formed at higher kinetic energies (i.e., more negative V_{oct} for the Agilent 8900). Thus, it is possible that the reactivity data presented here was collected using higher energies (more negative V_{oct}) than previous studies. However, previous work [29] does not list the parameters necessary for direct comparison.

Actinide reactivity with O_2 and O_2/He gas are shown in Fig. 1. All reactivity experiments using O_2/He were conducted with the addition of 8 mL·min^{-1} from the dedicated He line on the Agilent 8900 as this flow rate yielded the maximum improvement in sensitivity. Similar to CO_2, the actinides react with O_2 and O_2/He gas to form primarily MO^+ and MO_2^+ product ions, and higher flow rates shift product ions to higher order oxide products. However, unlike CO_2, the actinides tend to form higher order oxide products (MO_2^+) even at lower flow rates of O_2 and O_2/He, with <10% of signal remaining unreacted at M^+ for all O_2 and O_2/He flow rates tested (Fig. 1; Supporting Information). Plutonium$^+$ generally has a strong affinity to form the MO_2^+ product, although, at low flow rates of pure O_2 (0.225 mL·min^{-1}) significant amounts of Pu^+ (40%) react to form the MO^+ species (Fig. 1; Supporting Information). At higher O_2 flow rates (>0.90 mL·min^{-1}) <2% of Pu^+ forms the MO^+ species with all remaining Pu^+ reacting to form MO_2^+ ions. Americium$^+$ differs from the other actinides as it predominantly forms the MO^+ product with O_2 gas. Even at low O_2 flow rates (0.225 mL·min^{-1}) <5% of Am^+ remains on mass at M^+, and at higher flow rates the majority of Am^+ remains at the MO^+ product. However, at the maximum O_2 flow rate (1.5 mL·min^{-1}) a significant amount of Am^+ (~15%) forms MO_2^+ (Supporting Information). These observations are consistent with data reported elsewhere. [2, 6, 22, 24, 25, 31]

Actinide reactivity with O_2/He gas is broadly the same as O_2 gas, although, some differences are noticeable. At low flow rates (1.15 mL·min^{-1} O_2/He) a greater fraction (1-10%) of all the actinides remains on mass at M^+ (Supporting Information). Despite this, the fraction of Pu^+ that reacts to form the MO^+ product at low O_2/He flow rates is substantially reduced relative to pure O_2 (18.4% vs. 40%). This is likely attributed to the increased number of collisions facilitated by He. The other major difference observed with O_2/He gas is that Am^+ more completely reacts to form MO^+ (i.e. less Am^+ shifts to MO_2^+ even at high gas flows), with <3% of Am^+ shifting to the MO_2^+ product even at maximum O_2/He flow rates (Fig. 1; Supporting Information). Finally, total ion sensitivity improves for both Am^+ (+4-70%) and Pu^+ (+1-48%) when using O_2/He + He relative to pure O_2, with the one exception being Pu^+ at 0.45 mL·min^{-1} pure O_2, in which case a slight decrease in sensitivity (-~3%) is observed (Supporting Information). This general improvement in sensitivity is likely the result with collisional focusing associated with increased He in the CRC (Supporting Information).

Application to ^{241}Am-^{241}Pu separation

Directly measuring ^{241}Am-^{241}Pu by ICP-MS is complicated by two main factors, 1) matrix-derived polyatomic interferences (e.g., $^{207}Pb^{34}S^+$, $^{206}Pb^{35}Cl^+$, $^{209}Bi^{16}O_2^+$, $^{201}Hg^{40}Ar^+$ etc.) overlapping *m/z* = 241, and 2) $^{241}Am^+$ and $^{241}Pu^+$ being isobaric interferences of each other. Typically, these issues are mitigated through pre-treatment (i.e., chemical separation), to remove the majority of the matrix elements and separate $^{241}Am^+$ and $^{241}Pu^+$ from one another. [23] However, these interferences can be mitigated using a reaction gas if the gas both shifts $^{241}Am^+$ and $^{241}Pu^+$ to higher *m/z* products to reduce matrix-derived interferences (i.e., shifting away from *m/z* 241), and effectively separates $^{241}Am^+$ and $^{241}Pu^+$ by reacting to form different products. Based on the reactivity data presented above, CO_2 is not a suitable gas for this work because the majority of Am^+ remains on mass, and at higher flow rates Am^+ and Pu^+ tend to both form the MO^+ product and thus are not effectively separated. In contrast, with both O_2 and O_2/He, even at low flow rates (0.23 and 1.15 mL·min^{-1}, respectively) Am^+ and Pu^+ readily react to form different oxide products, resulting in a more efficient separation (Fig. 1). Therefore, in lieu of any pre-treatment, interferences are mitigated here by quantifying ^{241}Am and ^{241}Pu using the $^{241}Am^{16}O^+$ and $^{241}Pu^{16}O_2^+$ products at *m/z* = 257 and 273, respectively. Mixed O_2/He gas was selected for this work as improved sensitivity for AmO^+ (>3-60% depending on flow rate) and slightly better separation of AmO^+ and PuO_2^+ was observed relative to pure O_2 (Supporting Information).

The instrument parameters and gas flows were tuned to maximize $^{243}AmO^+$ and $^{242}PuO_2^+$ product formation, providing the best separation possible, while maintaining good sensitivity for both product ions (Table S1). With this approach, significant Am-Pu separation is achieved, with 98.2% of $^{243}Am^+$ forming $^{243}AmO^+$, and 98.5% of $^{242}Pu^+$ forming $^{242}PuO_2^+$. However, a small fraction of $^{243}Am^+$ and $^{242}Pu^+$ react to form $^{243}AmO_2^+$ (~1.2%) and $^{242}PuO^+$ (~1.3%), respectively. Although a small percentage, these products will lead to an inaccurate determination of ^{241}Am/^{241}Pu if left unaddressed. This issue becomes particularly apparent when analyzing samples with extreme differences in ^{241}Am and ^{241}Pu concentration where signal from $^{241}AmO^+$ or $^{241}PuO_2^+$ may be overwhelmed by the interfering product ion ($^{241}PuO^+$ or $^{241}AmO_2^+$). To address this issue, a standard-sample bracketing approach is implemented in which Am^+ and Pu^+ reactivity is assessed throughout each analysis using a standard containing $^{243}Am^+$ and $^{242}Pu^+$. The measured reactivity of $^{243}Am^+$ and $^{242}Pu^+$ is then used to correct for residual $^{241}PuO^+$ at *m/z* 257 and $^{241}AmO_2^+$ at *m/z* 273 using a mass balance approach. The following is an example of the correction applied to account for residual $^{241}PuO^+$ interference on $^{241}AmO^+$ at mass *m/z* = 257, beginning by defining the general mass balance equation as:

$$F_{MO}^{257} = \left({}^{MO}_{Am}R\right)\left(X_{Am}^{241}\right) + \left({}^{MO}_{Pu}R\right)\left(X_{Pu}^{241}\right) \quad \textit{Eq. 1}$$

Where F_{MO}^{257} is the measured fraction of signal (cps) at *m/z* = 257 relative to the total signal (cps) of product ions at *m/z* 257 and *m/z* 273, $\left({}^{MO}_{x}R\right)$ is the product formation ratio of MO^+ for $^{241}Am^+$ and $^{241}Pu^+$, respectively, and $\left(X_x^{241}\right)$ is the fraction of ^{241}Am and ^{241}Pu contributing to measured signal at *m/z* = 257. F_{MO}^{257} is defined as the following:

$$F_{MO}^{257} = \frac{MO^+\ (cps\ measured\ at\ m/z = 257)}{MO^+\ (cps\ measured\ at\ m/z = 257) + MO_2^+ (cps\ measured\ at\ m/z = 273)} \quad \textit{Eq.2}$$

The product formation ratio of MO^+ $\left({}^{MO}_{x}R\right)$ for ^{241}Am and ^{241}Pu, can be expressed as:

$${}^{MO}_{Pu}R = \frac{{}^{241}Pu^{16}O^+}{{}^{241}Pu^{16}O^+ + {}^{241}Pu^{16}O_2^+}, and \quad \textit{Eq. 3}$$

$${}^{MO}_{Am}R = \frac{{}^{241}Am^{16}O^+}{{}^{241}Am^{16}O^+ + {}^{241}Am^{16}O_2^+} \quad \textit{Eq. 4}$$

These values are determined using the reactivity of $^{243}Am^+$ and $^{242}Pu^+$ standards measured using a standard-sample bracketing approach:

$${}^{MO}_{Pu}R = \frac{{}^{242}Pu^{16}O^+ (cps\ at\ m/z = 258)}{{}^{242}Pu^{16}O^+ (cps\ at\ m/z = 258) + {}^{242}Pu^{16}O_2^+ (cps\ at\ m/z = 274)}, and \quad \textit{Eq. 5}$$

$${}^{MO}_{Am}R = \frac{{}^{243}Am^{16}O^+ (cps\ at\ m/z = 259)}{{}^{243}Am^{16}O^+ (cps\ at\ m/z = 259) + {}^{243}Am^{16}O_2^+ (cps\ at\ m/z = 275)} \quad \textit{Eq. 6}$$

With this information it is possible to solve the general mass balance equation (Eq.1) for the fraction of the measured signal at *m/z* 257 in the sample contributed from ^{241}Am (X_{Am}^{241}):

$$X_{Am}^{241} = \frac{\left(F_{MO}^{257} - {}^{MO}_{Pu}R\right)}{\left({}^{MO}_{Am}R - {}^{MO}_{Pu}R\right)} \quad \textit{Eq. 7}$$

As the total signal measured at *m/z* 257 is a combination of $^{241}Am^+$ and $^{241}Pu^+$, the fraction of signal from ^{241}Pu can be determined using the following:

$$X_{Pu}^{241} + X_{Am}^{241} = 1 \quad \textit{Eq. 8}$$

$$X_{Pu}^{241} = 1 - X_{Am}^{241} \quad \textit{Eq. 9}$$

The corrected total signal (summed signal of MO^+ and MO_2^+ in cps) contributed from ^{241}Am and ^{241}Pu is then determined using:

$$\left(cps\ {}^{241}Am^+\right)_{corr} = X_{Am}^{241}\left(MO^+ + MO_2^+\right) \quad \textit{Eq. 10}$$

$$\left(cps\ {}^{241}Pu^+\right)_{corr} = X_{Pu}^{241}\left(MO^+ + MO_2^+\right) \quad \textit{Eq. 11}$$

Where MO^+ and MO_2^+ are the measured signal intensities (cps) of the oxide products at m/z = 257 and m/z 273, respectively. The total efficiency of ^{241}Am and ^{241}Pu are corrected using the signal intensities ($MO^+ + MO_2^+$) from a single point calibration standard of ^{243}Am and ^{242}Pu, respectively. The ^{241}Am/^{241}Pu ratio is then used to determine the time since ^{241}Am-^{241}Pu separations using the following decay equation:

$$\frac{\lambda_2 N_2}{\lambda_1 N_1} = \frac{\lambda_2}{\lambda_2 - \lambda_1}\left(1 - e^{-(\lambda_2 - \lambda_1)t}\right) \quad \textit{Eq. 2}$$

Which can be rearranged to solve for time (t):

$$t = \frac{1}{(\lambda_1 - \lambda_2)} ln\left[1 - \frac{N_2}{N_1}\left(\frac{\lambda_2 - \lambda_1}{\lambda_1}\right)\right] \quad \textit{Eq. 3}$$

Where λ_1 and λ_2 are the decay constants for ^{241}Pu and ^{241}Am, respectively, and N_2/N_1 = ^{241}Am/^{241}Pu.

Direct determination of ^{241}Am/^{241}Pu ratios in unseparated samples

Two Pu isotopic standards, CRM-136 and CRM-137, were used to evaluate the developed method for the direct measurement of ^{241}Am/^{241}Pu in samples with no chemical pre-treatment. Each standard was measured at three concentrations of ^{241}Am and ^{241}Pu. Additionally, an aliquot of each Pu standard was spiked into NIST SRM 2711a (~1095 $\mu g \cdot g^{-1}$ solution) to assess method performance in high matrix samples. NIST SRM 2711a was selected specifically due to its high Pb content (0.14 wt%) which is a major source of polyatomic interferences on *m/z* 241 ($^{207}Pb^{34}S^+$, $^{206}Pb^{35}Cl^+$, $^{208}Pb^{16}O_2{}^1H^+$; Supporting Information). Total Pu concentrations ranged from 22-138 $pg \cdot g^{-1}$ and ~1204-5072 $pg \cdot g^{-1}$ for CRM-136 and CRM-137 solutions, respectively.

Results for ^{241}Am/^{241}Pu analysis are reported in Table 1. Reported ^{241}Am/^{241}Pu ratios and uncertainties are the average and standard deviation (1σ) of three replicate measurements of each solution. Regardless of sample matrix, measured ^{241}Am/^{241}Pu ratios for CRM-136 range from 11.94-12.28 (within 0.02-2.8% of expected) and the time since Pu-Am separation is calculated to be 54.07-54.63 years (May – Nov 1970), which overlaps the consensus model purification data of 5/23/1970. [37] Measured ^{241}Am/^{241}Pu ratios for CRM-137 range from 0.144 – 0.147, within 1.3-3.4% of the expected ratio of 0.149. These results yield a calculated time since Pu-Am separation of 2.78-2.84 years, equating to a separation date ranging from 2/14/2022 – 3/7/2022 (known separation date of 2/2/2022). A critical aspect of these results is that accurate determination of ^{241}Am/^{241}Pu ratios is achieved regardless of sample matrix and without any chemical separation. Better precision using methods similar to those presented here may be achieved using newly developed CRC-MC-ICP-MS instruments (i.e., Thermo

Scientific Neoma MS/MS and Nu Sapphire); however, Q-ICP-MS/MS provides better control over the reactions occurring in the CRC especially when dealing with high matrix. [48]

Table 1: Results of $^{241}Am/^{241}Pu$ analysis.

	^{241}Am	^{241}Pu		$^{241}Am/^{241}Pu$		Time since Am-Pu separation			
Sample*	[pg/g]	[pg/g]	Calculated	measured	error (%)	Age (yrs)	(+)	(-)	separation date
CRM-136	1.38	0.11	12.28	12.18 ± 0.41	-0.8%	54.46	0.04	0.04	7/4/1970
CRM-136	2.67	0.22	12.28	12.11 ± 0.38	-1.4%	54.34	0.04	0.04	8/16/1970
CRM-136	5.05	0.41	12.28	12.28 ± 0.27	0.02%	54.63	0.02	0.02	5/2/1970
CRM-136 + NIST 2711a	0.91	0.074	12.28	11.94 ± 0.18	-2.8%	54.07	0.03	0.03	11/23/1970
CRM-137	0.45	3.04	0.149	0.144 ± 0.002	-3.4%	2.78	0.65	0.67	3/7/2022
CRM-137	0.90	6.05	0.149	0.145 ± 0.002	-2.4%	2.81	0.61	0.63	2/25/2022
CRM-137	1.81	12.14	0.149	0.146 ± 0.001	-2.3%	2.82	0.42	0.43	2/24/2022
CRM-137 + NIST 2711a	0.58	3.92	0.149	0.147 ± 0.002	-1.3%	2.84	0.29	0.30	2/14/2022

*CRM-136 was separated between March/April 1970 and CRM-137 was separated on 2/2/2022. All solutions were measured 12/19/2024. Uncertanties in measured $^{241}Am/^{241}Pu$ ratios are the standard deviation (1σ) of three replicate measurements. Error = (measured-calculated)/calculated x 100.

Instrument detection limits for this method were determined to be 0.17 $fg \cdot g^{-1}$ and 0.25 $fg \cdot g^{-1}$ for $^{241}AmO^+$ (*m/z* 257) and $^{241}PuO_2^+$ (*m/z* 273), respectively. Detection limits were quantified using three times the standard deviation of 2% nitric acid blanks (n=3) measured throughout the analysis and sensitivity determined from ^{243}Am and ^{242}Pu standards. Method detection limits within the soil matrix were calculated to be 15.9 $fg \cdot g^{-1}$ and 9.8 $fg \cdot g^{-1}$ solution, or 14.5 $pg \cdot g^{-1}$ and 8.9 $pg \cdot g^{-1}$ soil, for ^{241}Am and ^{241}Pu, respectively. Method detection limits were determined by accounting for reactivity and sensitivity measured for $^{243}Am^+$ and $^{242}Pu^+$ standard solutions analyzed throughout the analysis (n=7).

The ability to measure $^{241}Am/^{241}Pu$ ratios will be dependent on the initial Pu concentration, the time since production or purification of Pu material (i.e., the time from ^{241}Am ingrowth) and the original abundance of ^{241}Pu (i.e., Pu isotopic composition). Analysis of old Pu materials will be limited by the ability to accurately analyze the remaining ^{241}Pu. Considering the first ever man-made Pu material was produced in December 1940, the largest possible $^{241}Am/^{241}Pu$ ratio for Pu material is ~52.15, if analyzed at the time of manuscript preparation (March 2025). Assuming a sample of this material had a starting isotopic composition similar to CRM-136, a minimum Pu concentration of ~30 $ng \cdot g^{-1}$ would be needed in the starting material (~30 $pg \cdot g^{-1}$ Pu in 1000x dilution) to have sufficient ^{241}Pu to exceed the calculated LOD of 9.8 $fg \cdot g^{-1}$. If the starting material contained a higher fraction of ^{241}Pu, then the amount of Pu necessary would be reduced. For example, if using the isotopic composition of CRM-137 (4.572 wt% ^{241}Pu), only ~3 $ng \cdot g^{-1}$ total Pu is needed in a material to ensure sufficient ^{241}Pu for measurement in a 1000x dilution.

Analysis of young Pu material will be a greater challenge, as there is limited time for ^{241}Am ingrowth, thus the ability to measure ^{241}Am becomes the limiting factor. For example, a material

containing 1 μg·g^{-1} total Pu with a starting isotopic composition similar to that of CRM-136 will contain 18 pg·g^{-1} ^{241}Am, with a ^{241}Am/^{241}Pu of 0.0009, after one week of ingrowth. A 1000x dilution (1000 μg·g^{-1}) of such a material would contain ~1 ng·g^{-1} total Pu, 20.05 pg·g^{-1} ^{241}Pu, and 18 fg·g^{-1} ^{241}Am, and thus should be directly measurable by this method as the ^{241}Am concentration exceeds the calculated LOD (15.9 fg·g^{-1}). However, if the starting material has a lower Pu concentration or lower abundance of ^{241}Pu a longer duration of ingrowth would be required for ^{241}Am concentrations to reach measurable levels by direct analysis. Thus, analysis of ^{241}Am/^{241}Pu ratios is directly dependent on the Pu concentration and isotopic composition of the initial sample.

Furthermore, if ^{241}Am and ^{241}Pu concentrations are above detection limit (>~16 fg·g^{-1}), accurate determination of extreme ^{241}Am/^{241}Pu ratios will be limited by the ability to correct for uncertainties associated with ^{241}Am$^+$ and ^{241}Pu$^+$ reactivity. For example, the ability to measure low ^{241}Am/^{241}Pu will be limited by ability to resolve small amount of ^{241}Am from ^{241}Pu. The fraction of ^{241}Am necessary to reliably resolve from residual ^{241}PuO$^+$ at *m/z* 257 can be calculated as the fraction ^{241}Am needed to be beyond three times the standard deviation of PuO$^+$ product formation, which is determined from replicate measurements (n=7) of ^{242}Pu standards throughout the analysis. The determined minimum fraction of ^{241}Am required can then be used to estimate a lower limit on the ^{241}Am/^{241}Pu ratio that can be reliably measured by this method. A similar exercise can be conducted to estimate an upper limit on ^{241}Am/^{241}Pu for old Pu materials. This exercise yields an estimated measurable range of ^{241}Am/^{241}Pu ratios of ~0.004 - 489, which equates to 0.08 – 132 years. The ^{241}Am/^{241}Pu ratio for the oldest known Pu material, produced in December of 1940, will not exceed the limitation of this method until ~2072. Therefore, analysis of the oldest produced Pu material should be achievable if ^{241}Pu concentrations of analyzed solutions exceed the limit of detection (~10 fg·g^{-1}). Analysis of young Pu material will be a greater challenge, as there is limited time for ^{241}Am ingrowth, thus the ability to separate ^{241}Am from ^{241}Pu becomes the limiting factor assuming ^{241}Am is above detection limits. Material with an age of 0.08 years, or 1 month, will have a ^{241}Pu/^{241}Am ratio of 243.9 resulting in a ^{241}PuO$^+$/^{241}AmO$^+$ ratio of 3.256 when accounting for reactivity. Correcting for a background that is 3 times the analyte signal would be possible but will impart a larger uncertainty on the final measurement. As such, it is not possible to place a uniform lower limit on the Pu concentration, the abundance of ^{241}Pu, or the age of Pu material required for direct analysis of ^{241}Am/^{241}Pu by this method.

The practicality of the method developed here will ultimately be driven by the target application. In situations where Pu concentration is not expected to be a limiting factor (i.e., dating of Pu materials)

direct analysis of $^{241}Am/^{241}Pu$ ratios in materials spanning from the oldest produced Pu material (December 1940) to materials on the order of weeks to months old should be achievable. In contrast, for materials with very low initial Pu and Am concentrations (i.e., $pg \cdot g^{-1}$ or less) a 1000x dilution would likely render Pu and Am concentration in the dilute solution too low for direct analysis. In which case a simplified column procedure to remove matrix components (i.e., major elements) and preconcentrate Pu and Am may be required. Importantly, this method is still valuable in such a scenario as Am and Pu do not need to be separated from one another prior to analysis. In summary, the method developed here using Q-ICP-MS/MS with O_2/He as a reaction gas allows for direct and accurate measurement of $^{241}Am/^{241}Pu$ ratios in simple and complex sample matrices without the need for chemical separation. These results highlight the ability of ICP-MS/MS techniques to facilitate rapid accurate actinide analysis in complex samples with a reduced need for chemical separations.

Conclusions

Actinide (Pa^+, Th^+, Np^+, U^+, Pu^+, Am^+, Cm^+) reactivity with CO_2, O_2, and O_2/He gas was assessed using Q-ICP-MS/MS. The primary products observed were MO^+ and MO_2^+ across all actinides and gases evaluated, with the exception being Am^+ with CO_2, which mainly remained unreacted at M^+. Additionally, increasing reaction gas flow rate (i.e., pressure) shifted reaction products to higher order oxide species (e.g., $M^+ \rightarrow MO^+$; $MO^+ \rightarrow MO_2^+$). The general actinide reactivity data were then used to develop a novel method using O_2/He gas to directly measure $^{241}Am/^{241}Pu$ ratios in the presence of complex sample matrices without the need for time consuming analyte separation techniques. The presented method circumvents matrix-derived polyatomic interferences (e.g., $^{208}Pb^{16}O_2H^+$, $^{206}Pb^{35}Cl^+$, etc.) by measuring both $^{241}Am^+$ and $^{241}Pu^+$ at an oxide product and resolves the isobaric interference of $^{241}Am^+$ and $^{241}Pu^+$ on one another by measuring $^{241}Am^+$ at *m/z* 257 ($^{241}Am^{16}O^+$) and $^{241}Pu^+$ at *m/z* 273 ($^{241}Pu^{16}O_2^+$). Measured $^{241}Am/^{241}Pu$ ratios were determined to be within <3.5% of the expected ratio for two Pu isotope standards (CRM-136 and CRM-137) within both simple and complex sample matrices containing ~1095 $\mu g \cdot g^{-1}$ soil (NIST SRM 2711a). Calculated dates for the times since Pu purification using measured $^{241}Am/^{241}Pu$ ratios overlap with, or are within weeks, of the known separation date for Pu isotope standards that underwent separation ca. 5/1970 (CRM-136) and 2/2/2022 (CRM-137), indicating this method can be used to rapidly and accurately determine the timing of Pu material production. To the authors' knowledge, this is the first method for direct simultaneous analysis of $^{241}Am/^{241}Pu$ in complex matrices without time-consuming front-end chemistry. This work highlights the utility of using ICP-

MS/MS techniques to facilitate rapid accurate actinide analysis in complex samples with a reduced, or even eliminated, need for chemical separations.

Acknowledgements

This work was funded by the U.S. Department of Energy's National Nuclear Security Administration, Office of Defense Nuclear Nonproliferation Research and Development, and by PNNL's Laboratory Directed Research and Development program. Pacific Northwest National Laboratory is operated by Battelle Memorial Institute for the U.S. Department of Energy (DOE) under contract number DE-AC05-76RL01830.

Supporting information

1. Tuning parameters for actinide reactivity experiments and optimized tuning parameters for $^{241}Am/^{241}Pu$ measurements
2. Flow rates and gas lines used for actinide reactivity experiments
3. Actinide products measured in standards at various gas flows ($mL \cdot min^{-1}$) with CO_2, O_2, and O_2/He gas
4. He gas effects on ion transmission
5. NIST SRM 2711a mass scan in single quad mode from *m/z* 229-244
6. Expanded discussion of general reactivity of actinide ions with CO_2, O_2, and O_2/He gas

References

(1) Gourgiotis, A.; Granet, M.; Isnard, H.; Nonell, A.; Gautier, C.; Stadelmann, G.; Aubert, M.; Durand, D.; Legand, S.; Chartier, F. Simultaneous uranium/plutonium separation and direct isotope ratio measurements by using CO2 as the gas in a collision/reaction cell based MC-ICPMS. *Journal of Analytical Atomic Spectrometry* **2010**, *25* (12). DOI: 10.1039/c0ja00092b.

(2) Kazama, H.; Konashi, K.; Suzuki, T.; Koyama, S.-i.; Maeda, K.; Sekio, Y.; Onishi, T.; Abe, C.; Shikamori, Y.; Nagai, Y. Reaction of Np, Am, and Cm ions with CO_2 and O_2 in a reaction cell in triple quadrupole inductively coupled plasma mass spectrometry. *Journal of Analytical Atomic Spectrometry* **2023**, *38* (8), 1676-1681. DOI: 10.1039/d3ja00136a.

(3) Kaszuba, J. P.; Runde, W. H. The Aqueous Geochemistry of Neptunium: Dynamic Control of Soluble Concentrations with Applications to Nuclear Waster Disposal. *Environmental Science & Technology* **1999**, *33* (24), 4427-4433.

(4) Boulyga, S. F.; Zoriy, M.; Ketterer, M. E.; Becker, J. S. Depth profiling of Pu, ^{241}Am and ^{137}Cs in soils from southern Belarus measured by ICP-MS and alpha and gamma spectrometry. *J Environ Monit* **2003**, *5* (4), 661-666. DOI: 10.1039/b303621a.

(5) Diez-Fernandez, S.; Jaegler, H.; Bresson, C.; Chartier, F.; Evrard, O.; Hubert, A.; Nonell, A.; Pointurier, F.; Isnard, H. A new method for determining ^{236}U/^{238}U isotope ratios in environmental samples by means of ICP-MS/MS. *Talanta* **2020**, *206*, 120221. DOI: 10.1016/j.talanta.2019.120221.

(6) Jaegler, H.; Gourgiotis, A. A new milestone for ultra-low ^{236}U/^{238}U isotope ratio measurements by ICP-MS/MS. *Journal of Analytical Atomic Spectrometry* **2023**, *38* (10), 1914-1919. DOI: 10.1039/d3ja00175j.

(7) Tanner, S. D.; Li, C.; Vais, V.; Baranov, V. I.; Bandura, D. R. Chemical Resolution of Pu^+ from U^+ and Am^+ Using a Band-Pass Reaction Cell Inductively Coupled Plasma Mass Spectrometer. *Anal Chem* **2004**, *76*, 3042-3048.

(8) Wolf, S. F. Trace Analysis of Actinides in Geological, Environmental, and Biological Matrices. *The Chemistry of the Actinide and Transactinide Elements*, Morss, L. R., Edelstein, N. M., Fuger, J. Eds.; Springer Netherlands, 2006; pp 3273-3338.

(9) Varga, Z.; Wallenius, M.; Krachler, M.; Rauff-Nisthar, N.; Fongaro, L.; Knott, A.; Nicholl, A.; Mayer, K. Trends and perspectives in Nuclear Forensic Science. *TrAC Trends in Analytical Chemistry* **2022**, *146*. DOI: 10.1016/j.trac.2021.116503.

(10) Wang, W.; Xu, J.; Xi, R.; Guo, S.; Su, Y.; Fang, S.; Zhang, H.; Wang, Y.; Fan, J.; Feng, L.; et al. Precise and accurate isotopic analysis of uranium and thorium in uranium ore concentrates using ICP-MS and their age dating for nuclear forensic analysis. *Journal of Analytical Atomic Spectrometry* **2024**, *39* (1), 178-189. DOI: 10.1039/d3ja00196b.

(11) Hobbs, K. P.; French, A. D.; Melby, K. M.; Bylaska, E. J.; Harouaka, K.; Cox, R. M.; Arnquist, I. J.; Beck, C. L. Assessing Gas-Phase Ion Reactivity of 50 Elements with NO and the Direct Application for ^{239}Pu in Complex Matrices Using ICP-MS/MS. *Anal Chem* **2024**, *96* (15), 5807-5814. DOI: 10.1021/acs.analchem.3c04774.

(12) Vajda, N.; Kim, C. K. Determination of transuranium isotopes (Pu, Np, Am) by radiometric techniques: a review of analytical methodology. *Anal Chem* **2011**, *83* (12), 4688-4719. DOI: 10.1021/ac2008288.

(13) Hou, X.; Roos, P. Critical comparison of radiometric and mass spectrometric methods for the determination of radionuclides in environmental, biological and nuclear waste samples. *Anal Chim Acta* **2008**, *608* (2), 105-139. DOI: 10.1016/j.aca.2007.12.012.

(14) Aggarwal, S. K. Thermal ionisation mass spectrometry (TIMS) in nuclear science and technology – a review. *Analytical Methods* **2016**, *8* (5), 942-957. DOI: 10.1039/c5ay02816g.

(15) Becker, J. S. State-of-the-art and progress in precise and accurate isotope ratio measurements by ICP-MS and LA-ICP-MS : Plenary Lecture. *J. Anal. At. Spectrom.* **2002**, *17* (9), 1172-1185. DOI: 10.1039/b203028b.
(16) Balaram, V.; Rahaman, W.; Roy, P. Recent advances in MC-ICP-MS applications in Earth and environmental sciences: Challenges and solutions. *Geosystems and Geoenvironment* **2022**, *1* (2). DOI: 10.1016/j.geogeo.2021.100019.
(17) Ammann, A. A. Inductively coupled plasma mass spectrometry (ICP MS): a versatile tool. *J Mass Spectrom* **2007**, *42* (4), 419-427. DOI: 10.1002/jms.1206.
(18) Walder, A. J.; Freedman, P. A. Isotopic Ratio Measurement Using a Double Focusing Magnetic Sector Mass Analyser with an Inductively Couple Plasma as an Ion Source. *Journal of Analytical Atomic Spectrometry* **1992**, *7*, 571-575. DOI: https://doi.org/10.1039/JA9920700571.
(19) Hou, X.; Zhang, W.; Wang, Y. Determination of Femtogram-Level Plutonium Isotopes in Environmental and Forensic Samples with High-Level Uranium Using Chemical Separation and ICP-MS/MS Measurement. *Anal Chem* **2019**, *91* (18), 11553-11561. DOI: 10.1021/acs.analchem.9b01347.
(20) Huang, Z.; Hou, X.; Zhao, X. Rapid and Simultaneous Determination of ^{238}Pu, ^{239}Pu, ^{240}Pu, and ^{241}Pu in Samples with High-Level Uranium Using ICP-MS/MS and Extraction Chromatography. *Anal Chem* **2023**, *95* (34), 12931-12939. DOI: 10.1021/acs.analchem.3c02526.
(21) Dowell, S. M.; Barlow, T. S.; Chenery, S. R.; Humphrey, O. S.; Isaboke, J.; Blake, W. H.; Osano, O.; Watts, M. J. Optimisation of plutonium separations using TEVA cartridges and ICP-MS/MS analysis for applicability to large-scale studies in tropical soils. *Anal Methods* **2023**, *15* (34), 4226-4235. DOI: 10.1039/d3ay01030a.
(22) Zhang, W.; Lin, J.; Fang, S.; Li, C.; Yi, X.; Hou, X.; Chen, N.; Zhang, H.; Xu, Y.; Dang, H.; et al. Determination of ultra-trace level plutonium isotopes in soil samples by triple-quadrupole inductively coupled plasma-mass spectrometry with mass-shift mode combined with UTEVA chromatographic separation. *Talanta* **2021**, *234*, 122652. DOI: 10.1016/j.talanta.2021.122652.
(23) Zhang, W.; Zhang, H.; Fang, S.; Hou, X.; Zhang, L.; Dang, H.; Yi, X.; Zhai, S.; Wang, W.; Xu, J. Determination of ultra-low level ^{241}Am in soil and sediment using chemical separation and triple quadrupole inductively coupled plasma mass spectrometry measurement with He-NH_3 as collision-reaction gas. *Spectrochimica Acta Part B: Atomic Spectroscopy* **2021**, *178*. DOI: 10.1016/j.sab.2021.106113.
(24) Jaegler, H.; Gourgiotis, A.; Steier, P.; Golser, R.; Diez, O.; Cazala, C. Pushing Limits of ICP-MS/MS for the Determination of Ultralow ^{236}U/^{238}U Isotope Ratios. *Anal Chem* **2020**, *92* (11), 7869-7876. DOI: 10.1021/acs.analchem.0c01121.
(25) Suzuki, T.; Yamamura, T.; Abe, C.; Konashi, K.; Shikamori, Y. Actinide molecular ion formation in collision/reaction cell of triple quadrupole ICP-MS/MS and its application to quantitative actinide analysis. *Journal of Radioanalytical and Nuclear Chemistry* **2018**, *318* (1), 221-225. DOI: 10.1007/s10967-018-6095-7.
(26) Bradley, V. C.; Ticknor, B. W.; Dunlap, D. R.; Zirakparvar, N. A.; Metzger, S. C.; Hexel, C. R.; Manard, B. T. Microextraction-TQ-ICP-MS for the Direct Analysis of U and Pu from Cotton Swipes. *Anal Chem* **2023**, *95* (43), 15867-15874. DOI: 10.1021/acs.analchem.3c01022.
(27) Epov, V. N.; Benkhedda, K.; Cornett, R. J.; Evans, R. D. Rapid determination of plutonium in urine using flow injection on-line preconcentration and inductively coupled plasma mass spectrometry. *Journal of Analytical Atomic Spectrometry* **2005**, *20* (5). DOI: 10.1039/b501218j.
(28) Cox, R. M.; Harouaka, K.; Citir, M.; Armentrout, P. B. Activation of $CO(_2)$ by Actinide Cations (Th^+, U^+, Pu^+, and Am^+) as Studied by Guided Ion Beam and Triple Quadrupole Mass Spectrometry. *Inorg Chem* **2022**, *61* (21), 8168-8181. DOI: 10.1021/acs.inorgchem.2c00447.

(29) Tiong, L. Y. D.; Tan, S. In situ determination of ^{238}Pu in the presence of uranium by triple quadrupole ICP-MS (ICP-QQQ-MS). *Journal of Radioanalytical and Nuclear Chemistry* **2019**, *322* (2), 399-406. DOI: 10.1007/s10967-019-06695-3.
(30) Childs, D. A.; Hill, J. G. The use of carbon dioxide as the reaction cell gas for the separation of uranium and plutonium in quadrupole inductively coupled plasma mass spectrometry (ICP-MS) for nuclear forensic samples. *Journal of Radioanalytical and Nuclear Chemistry* **2018**, *318* (1), 139-148. DOI: 10.1007/s10967-018-5973-3.
(31) Matsueda, M.; Kawakami, T.; Koarai, K.; Terashima, M.; Fujiwara, K.; Iijima, K.; Furukawa, M.; Takagai, Y. Using CO_2 Reactions to Achieve Mass-spectrometric Discrimination in Simultaneous Plutonium-isotope Speciation with Inductively Coupled Plasma–Tandem Mass Spectrometry. *Chemistry Letters* **2022**, *51* (7), 678-682. DOI: 10.1246/cl.220160.
(32) Hobbs, K. P.; French, A. D.; Scott, S. R.; RisenHuber, M. A.; Haney, M. M.; Arnquist, I. J.; Herman, S. M.; Beck, C. L. Rapid analysis of ^{237}Np and Pu isotopes in unseparated sample matrices using ICP-MS/MS. *Talanta* **2025**, *287*, 127666. DOI: 10.1016/j.talanta.2025.127666.
(33) Zhang, H.; Hou, X.; Qiao, J.; Lin, J. Determination of ^{241}Am in Environmental Samples: A Review. *Molecules* **2022**, *27* (14). DOI: 10.3390/molecules27144536.
(34) Varga, B.; Tarjan, S. Determination of ^{241}Pu in the environmental samples. *Appl Radiat Isot* **2008**, *66* (2), 265-270. DOI: 10.1016/j.apradiso.2007.09.011.
(35) UNSCEAR. *Sources and Effects of Ionizing Radiation. Report to the General Assembly, with Scientific Annexes*; United Nations Scientific Committee on the Effects of Atomic Radiation, 2000.
(36) Aggarwal, S. K. A review on the mass spectrometric studies of americium: Present status and future perspective. *Mass Spectrom Rev* **2018**, *37* (1), 43-56. DOI: 10.1002/mas.21506.
(37) Mathew, K.; Kayzar-Boggs, T.; Varga, Z.; Gaffney, A.; Denton, J.; Fulwyler, J.; Garduno, K.; Gaunt, A.; Inglis, J.; Keller, R.; et al. Intercomparison of the Radio-Chronometric Ages of Plutonium-Certified Reference Materials with Distinct Isotopic Compositions. *Anal Chem* **2019**, *91* (18), 11643-11652. DOI: 10.1021/acs.analchem.9b02156.
(38) Goldstein, S. J.; Hinrichs, K. A.; Nunn, A. J.; Gurganus, D. W.; Amato, R. S.; Oldham, W. J. Sequential chemical separations and multiple ion counting ICP-MS for ^{241}Pu–^{241}Am–^{237}Np dating of environmental collections on a single aliquot. *Journal of Radioanalytical and Nuclear Chemistry* **2018**, *318* (1), 695-701. DOI: 10.1007/s10967-018-6045-4.
(39) Zhang, L.; Vassileva, E. Determination of ultra-trace level ^{241}Am in marine sediment and seawater by combining TK200-TK221 tandem-column extraction chromatography and SF ICP-MS. *Talanta* **2024**, *271*, 125724. DOI: 10.1016/j.talanta.2024.125724.
(40) Agarande, M.; Benzoubir, S.; Bouisset, P.; Calmet, D. Determination of ^{241}Am in sediments by isotope dilution high resolution inductively coupled plasma mass spectrometry (ID HR ICP-MS). *Applied Radiation and Isotopes* **2001**, *55*, 161-165.
(41) Zheng, J.; Yamada, M. Isotope Dilution Sector-Field Inductively Coupled Plasma Mass Spectrometry Combined with Extraction Chromatography for Rapid Determination of 241Am *Journal of Oceanography* **2008**, *64*, 541-550.
(42) Krachler, M.; Alvarez-Sarandes, R.; Van Winckel, S. Elemental and isotopic analysis of americium in non-separated spent fuels using high resolution ICP-OES and sector field ICP-MS. *Journal of Analytical Atomic Spectrometry* **2014**, *29* (5). DOI: 10.1039/c4ja00068d.
(43) Xiong, K.; Bu, W.; Ni, Y.; Liu, X.; Zheng, J.; Aono, T.; Yang, C.; Hu, S. Rapid monitoring of ^{241}Am in small amount of sediment samples by combining extraction chromatography for highly efficient separation of interfering and matrix elements and ICP-MS/MS measurement. *Microchemical Journal* **2023**, *190*. DOI: 10.1016/j.microc.2023.108581.
(44) Peng, C.; Sun, J.; Zhang, F.; Xing, S.; Liu, X.; Chen, C.; Hou, X.; Shi, K.; Wu, W. Simultaneous Determination of Transuranium Radionuclides in Urine by Tandem Quadrupole ICP-MS/MS with Mass-

Shift Mode Combined with Chemical Separation. *Anal Chem* **2024**, *96* (6), 2514-2523. DOI: 10.1021/acs.analchem.3c04699.
(45) Zhang, W.; Lin, J.; Zhang, H.; Fang, S.; Li, C.; Yi, X.; Dang, H.; Xu, Y.; Wang, W.; Xu, J. Determination of ultra-trace level ^{241}Am in soil by triple-quadrupole inductively coupled plasma-mass spectrometry with mass-shift mode combined with chemical separation. *Journal of Analytical Atomic Spectrometry* **2022**, *37* (5), 1044-1052. DOI: 10.1039/d1ja00403d.
(46) Harouaka, K.; Melby, K.; Bylaska, E. J.; Cox, R. M.; Eiden, G. C.; French, A.; Hoppe, E. W.; Arnquist, I. J. Gas-Phase Ion-Molecule Interactions in a Collision Reaction Cell with ICP-MS/MS: Investigations with CO_2 as the Reaction Gas. *Geostandards and Geoanalytical Research* **2022**, *46* (3), 387-399. DOI: 10.1111/ggr.12429.
(47) French, A. D.; Melby, K. M.; Hobbs, K. P.; Cox, R. M.; Eiden, G.; Hoppe, E. W.; Arnquist, I. J.; Harouaka, K. The importance of ion kinetic energy for interference removal in ICP-MS/MS. *Talanta* **2024**, *272*, 125799. DOI: 10.1016/j.talanta.2024.125799.
(48) Scott, S. R.; Hobbs, K. P.; French, A. D.; Arnquist, I. J.; Alcantar Anguiano, S.; Sullivan, D. L.; Herman, S. M. Uranium isotopic analysis in unpurified solutions by ICP-MS. *Journal of Analytical Atomic Spectrometry* **2024**, *39* (8), 2106-2115. DOI: 10.1039/d4ja00130c.

Supporting Information

An evaluation of actinide reactivity with CO_2, O_2, and O_2/He gases using ICP-MS/MS: Application to simultaneous measurement of $^{241}Am/^{241}Pu$ ratios in unseparated complex matrices

Authors: Tyler D. Schlieder[1], *Kirby P. Hobbs[1], Amanda D. French[1]*, Lee H. Hughes[1], Isaac J. Arnquist[1], Chelsie Beck[1]*

[1]Pacific Northwest National Laboratory, Richland, WA, 99352 USA

Table of Contents

Table S1. Tuning parameters for actinide reactivity experiments and optimized tuning parameters for $^{241}Am/^{241}Pu$ measurements 2

Table S2. Flow rates and gas lines used for actinide reactivity experiments.....3

Table S3.x. Actinide products measured in standards at various gas flows ($mL \cdot min^{-1}$) with CO_2, O_2, and O_2/He gas.....4-9

Figure S1. He gas effects on ion transmission 10

Figure S2. NIST SRM 2711a mass scan in single quad mode from *m/z* 229-244.....11

Text S1. Discussion on general reactivity of actinide ions with CO_2, O_2, and O_2/He gas 12

Table S1. Tuning parameters for actinide reactivity experiments and optimized tuning parameters for $^{241}Am/^{241}Pu$ measurements.

Tuning Parameter	Reactivity Experiments	$^{241}Am/^{241}Pu$ application
RF Power	1600 W	1600 W
RF Matching	1.20 V	1.20 V
Sample Depth	3.0 mm	3.0 mm
Nebulizer Gas	0.85 L/min	0.82 L/min
Spray Chamber Temperature	2°C	2°C
Makeup Gas	0.23 L/min	0.23 L/min
Auxiliary Gas	0.9 L/min	0.9 L/min
Plasma Gas	18.0 L/min	18.0 L/min
Extract 1	6.5 V	5.5 V
Extract 2	-250.0 V	-235.0 V
Omega Bias	-200 V	-200 V
Omega Lens	20.0 V	19.0 V
Q1 Entrance	0.0 V	3.0 V
Q1 Exit	3.0 V	4.0 V
Cell Focus	-10.0 V	-10.0 V
Cell Entrance	-80 V	-120 V
Cell Exit	-80 V	-80 V
Deflect	20.0 V	-8.0 V
Plate Bias	-70 V	-60 V
Q1 Bias	-1.0 V	-1.0 V
OctP Bias	-8.0 V	-12.0 V
Axial Acceleration	0.0 V	2.0 V
OctP RF	180 V	180 V
Energy Discrimination	5.0 V	-11.0 V
Wait Time Offset	0 msec	0 msec

Table S2. Flow rates and gas lines used for actinide reactivity experiments.

	Gas Flow Rate [sccm]		
Flow rate [%]	**CO_2 (4th cell)**	**O_2 (4th cell)**	**10% O_2-He (3rd cell)**
0	0	0	0
15	0.16	0.23	1.15
30	0.32	0.45	2.31
60	0.63	0.9	4.62
100	1.05	1.5	7.69

Table S3.1. Actinide products measured in standards at various gas flows (mL·min^{-1}) using CO_2 gas.

	Pure CO_2			0.16 mL·min^{-1}		0.32 mL·min^{-1}		0.63 mL·min^{-1}		1.05 mL·min^{-1}	
Std	**Q1**	**Q2**	**Species**	**CPS**	**%**	**CPS**	**%**	**CPS**	**%**	**CPS**	**%**
0.5 ppt	231	231	Pa^+	17	1.2%	0	0.0%	0	0.0%	0	0.0%
^{231}Pa		243	PaC^+	0	0.0%	0	0.0%	0	0.0%	0	0.0%
		247	PaO^+	224	16.3%	33	2.5%	0	0.0%	0	0.0%
		248	$PaOH^+$	0	0.0%	0	0.0%	0	0.0%	0	0.0%
		249	$PaOH_2^+$	7	0.5%	0	0.0%	0	0.0%	0	0.0%
		263	PaO_2^+	1128	82.0%	1275	96.7%	410	99.2%	33	100.0%
		264	PaO_2H^+	0	0.0%	3	0.3%	3	0.8%	0	0.0%
		265	$PaO_2H_2^+$	0	0.0%	7	0.5%	0	0.0%	0	0.0%
		total cps		1375		1318		414		33	
1 ppb	232	232	Th^+	3704	0.6%	143	0.0%	0	0.0%	0	0.0%
^{232}Th		244	ThC^+	0	0.0%	0	0.0%	0	0.0%	0	0.0%
		248	ThO^+	295617	47.2%	77986	13.2%	561	0.4%	7	0.1%
		249	$ThOH^+$	83	0.0%	23	0.0%	0	0.0%	0	0.0%
		250	$ThOH_2^+$	611	0.1%	137	0.0%	0	0.0%	0	0.0%
		264	ThO_2^+	320956	51.3%	503600	84.9%	124733	94.1%	3177	71.0%
		265	ThO_2H^+	3574	0.6%	8872	1.5%	6665	5.0%	1278	28.6%
		266	$ThO_2H_2^+$	1235	0.2%	2076	0.4%	537	0.4%	10	0.2%
		total cps		625781		592837		132496		4472	
1 ppt	237	237	Np^+	17	3.4%	0	0.0%	0	0.0%	0	0.0%
^{237}Np		249	NpC^+	3	0.7%	0	0.0%	0	0.0%	0	0.0%
		253	NpO^+	450	93.1%	557	94.9%	304	91.9%	90	87.1%
		254	$NpOH^+$	3	0.7%	0	0.0%	0	0.0%	0	0.0%
		255	$NpOH_2^+$	0	0.0%	0	0.0%	3	1.0%	0	0.0%
		269	NpO_2^+	10	2.1%	10	1.7%	7	2.0%	10	9.7%
		270	NpO_2H^+	0	0.0%	17	2.8%	17	5.0%	3	3.2%
		271	$NpO_2H_2^+$	0	0.0%	3	0.6%	0	0.0%	0	0.0%
		total cps		484		587		330		103	
1 ppb	238	238	U^+	10448	1.7%	501	0.1%	3	0.0%	0	0.0%
^{238}U		250	UC^+	3	0.0%	0	0.0%	0	0.0%	0	0.0%
		254	UO^+	513667	84.8%	356544	58.2%	22631	10.2%	123	0.4%
		255	UOH^+	204	0.0%	130	0.0%	13	0.0%	0	0.0%
		256	UOH_2^+	924	0.2%	744	0.1%	50	0.0%	0	0.0%

		270	UO_2^+	79870	13.2%	253682	41.4%	198043	89.3%	30149	99.1%
		271	UO_2H^+	110	0.0%	280	0.0%	187	0.1%	23	0.1%
		272	$UO_2H_2^+$	370	0.1%	1141	0.2%	741	0.3%	120	0.4%
		total cps		605597		613023		221668		30416	
1 ppt	242	242	Pu^+	360	50.9%	100	13.5%	13	3.7%	0	0.0%
^{242}Pu		254	PuC^+	0	0.0%	0	0.0%	0	0.0%	0	0.0%
		258	PuO^+	347	49.1%	641	86.5%	344	96.3%	137	93.2%
		259	$PuOH^+$	0	0.0%	0	0.0%	0	0.0%	0	0.0%
		260	$PuOH_2^+$	0	0.0%	0	0.0%	0	0.0%	0	0.0%
		274	PuO_2^+	0	0.0%	0	0.0%	0	0.0%	10	6.8%
		275	PuO_2H^+	0	0.0%	0	0.0%	0	0.0%	0	0.0%
		total cps		707		741		357		147	
1 ppt	243	243	Am^+	585	92.9%	545	77.5%	345	69.7%	160	67.6%
^{243}Am		255	AmC^+	0	0.0%	2	0.2%	0	0.0%	0	0.0%
		259	AmO^+	43	6.9%	157	22.3%	145	29.3%	73	31.0%
		260	$AmOH^+$	0	0.0%	0	0.0%	0	0.0%	0	0.0%
		261	$AmOH_2^+$	2	0.3%	0	0.0%	2	0.3%	0	0.0%
		275	AmO_2^+	0	0.0%	0	0.0%	3	0.7%	3	1.4%
		total cps		630		703		495		237	
0.5 ppt	248	248	Cm^+	73	19.6%	30	7.1%	2	0.7%	0	0.0%
^{248}Cm		260	CmC^+	0	0.0%	0	0.0%	0	0.0%	0	0.0%
		264	CmO^+	300	80.0%	388	92.5%	243	99.3%	50	100.0%
		265	$CmOH^+$	2	0.4%	2	0.4%	0	0.0%	0	0.0%
		266	$CmOH_2^+$	2	0.4%	2	0.4%	0	0.0%	0	0.0%
		total cps		376		421		245		50	

Table S3.2. Actinide products measured in standards at various gas flows (mL·min^{-1}) using O_2 gas.

	Pure O_2			0.225 mL·min^{-1}		0.45 mL·min^{-1}		0.90 mL·min^{-1}		1.50 mL·min^{-1}	
Std	**Q1**	**Q2**	**Species**	**CPS**	**%**	**CPS**	**%**	**CPS**	**%**	**CPS**	**%**
0.5 ppt	231	231	Pa^+	0	0.0%	0	0.0%	0	0.0%	0	0.0%
^{231}Pa		243	PaC^+	0	0.0%	0	0.0%	0	0.0%	0	0.0%
		247	PaO^+	30	3.5%	0	0.0%	0	0.0%	0	0.0%
		248	$PaOH^+$	0	0.0%	3	0.3%	0	0.0%	0	0.0%
		249	$PaOH_2^+$	0	0.0%	0	0.0%	0	0.0%	0	0.0%
		263	PaO_2^+	818	96.5%	1101	99.4%	697	100.0%	207	100.0%
		264	PaO_2H^+	0	0.0%	0	0.0%	0	0.0%	0	0.0%
		265	$PaO_2H_2^+$	0	0.0%	3	0.3%	0	0.0%	0	0.0%
		total cps		848		1108		697		207	
1 ppb	232	232	Th^+	270	0.1%	3	0.0%	3	0.0%	0	0.0%
^{232}Th		244	ThC^+	0	0.0%	0	0.0%	0	0.0%	0	0.0%
		248	ThO^+	113969	28.3%	29282	6.1%	894	0.3%	7	0.0%
		249	$ThOH^+$	60	0.0%	3	0.0%	0	0.0%	0	0.0%
		250	$ThOH_2^+$	254	0.1%	33	0.0%	0	0.0%	0	0.0%
		264	ThO_2^+	285990	71.0%	442253	92.5%	265046	96.2%	62857	91.6%
		265	ThO_2H^+	994	0.2%	4572	1.0%	8592	3.1%	5557	8.1%
		266	$ThO_2H_2^+$	1218	0.3%	1722	0.4%	1061	0.4%	234	0.3%
		total cps		402756		477869		275597		68655	
1 ppt	237	237	Np^+	0	0.0%	0	0.0%	0	0.0%	0	0.0%
^{237}Np		249	NpC^+	0	0.0%	0	0.0%	0	0.0%	0	0.0%
		253	NpO^+	47	12.3%	3	0.7%	0	0.0%	0	0.0%
		254	$NpOH^+$	0	0.0%	0	0.0%	0	0.0%	0	0.0%
		255	$NpOH_2^+$	0	0.0%	0	0.0%	0	0.0%	0	0.0%
		269	NpO_2^+	317	83.3%	470	97.9%	310	97.9%	123	97.4%
		270	NpO_2H^+	17	4.4%	0	0.0%	3	1.1%	3	2.6%
		271	$NpO_2H_2^+$	0	0.0%	7	1.4%	3	1.1%	0	0.0%
		total cps		380		480		317		127	
1 ppb	238	238	U^+	427	0.1%	7	0.0%	0	0.0%	0	0.0%
^{238}U		250	UC^+	0	0.0%	0	0.0%	0	0.0%	0	0.0%
		254	UO^+	20743	4.8%	1555	0.3%	47	0.0%	3	0.0%
		255	UOH^+	20	0.0%	0	0.0%	0	0.0%	0	0.0%
		256	UOH_2^+	23	0.0%	0	0.0%	0	0.0%	0	0.0%

		270	UO_2^+	410155	94.7%	553259	99.3%	362210	99.5%	108995	99.6%
		271	UO_2H^+	314	0.1%	380	0.1%	260	0.1%	80	0.1%
		272	$UO_2H_2^+$	1645	0.4%	2162	0.4%	1422	0.4%	394	0.4%
		total cps		433327		557363		363938		109472	
1 ppt ^{242}Pu	242	242	Pu^+	0	0.0%	0	0.0%	0	0.0%	0	0.0%
		254	PuC^+	0	0.0%	0	0.0%	0	0.0%	0	0.0%
		258	PuO^+	220	40.0%	47	7.7%	7	1.8%	0	0.0%
		259	$PuOH^+$	0	0.0%	0	0.0%	0	0.0%	0	0.0%
		260	$PuOH_2^+$	3	0.6%	0	0.0%	0	0.0%	0	0.0%
		274	PuO_2^+	327	59.4%	561	92.3%	357	98.2%	197	100.0%
		275	PuO_2H^+	0	0.0%	0	0.0%	0	0.0%		0.0%
		total cps		551		607		364		197	
1 ppt ^{243}Am	243	243	Am^+	15	2.9%	2	0.2%	0	0.0%	0	0.0%
		255	AmC^+	0	0.0%	0	0.0%	0	0.0%	0	0.0%
		259	AmO^+	491	95.2%	670	97.6%	441	93.0%	210	84.6%
		260	$AmOH^+$	0	0.0%	0	0.0%	0	0.0%	0	0.0%
		261	$AmOH_2^+$	2	0.3%	3	0.5%	3	0.7%	0	0.0%
		275	AmO_2^+	8	1.6%	12	1.7%	30	6.3%	38	15.4%
		total cps		516		686		475		248	
1 ppt ^{248}Cm	248	248	Cm^+	18	5.4%	2	0.4%	0	0.0%	0	0.0%
		260	CmC^+	2	0.5%	0	0.0%	0	0.0%	0	0.0%
		264	CmO^+	320	93.7%	391	99.6%	315	98.4%	162	100.0%
		265	$CmOH^+$	2	0.5%	0	0.0%	2	0.5%	0	0.0%
		266	$CmOH_2^+$	0	0.0%	0	0.0%	3	1.0%	0	0.0%
		total cps		342		393		320		162	

Table S3.3. Actinide products measured in standards at various gas flows (mL·min^{-1}) using O_2/He gas.

	10% O_2/He			1.15 mL·min^{-1}		2.31 mL·min^{-1}		4.62 mL·min^{-1}		7.69 mL·min^{-1}	
Std	**Q1**	**Q2**	**Species**	**CPS**	**%**	**CPS**	**%**	**CPS**	**%**	**CPS**	**%**
0.5 ppt	231	231	Pa^+	20	1.6%	0	0.0%	0	0.0%	0	0.0%
^{231}Pa		243	PaC^+	0	0.0%	0	0.0%	0	0.0%	0	0.0%
		247	PaO^+	50	3.9%	3	0.3%	0	0.0%	0	0.0%
		248	$PaOH^+$	3	0.3%	0	0.0%	0	0.0%	0	0.0%
		249	$PaOH_2^+$	0	0.0%	0	0.0%	0	0.0%	0	0.0%
		263	PaO_2^+	1181	93.2%	1011	99.0%	617	99.5%	297	97.8%
		264	PaO_2H^+	7	0.5%	0	0.0%	3	0.5%	7	2.2%
		265	$PaO_2H_2^+$	7	0.5%	7	0.7%	0	0.0%	0	0.0%
		total cps		1268		1021		621		304	
1 ppb	232	232	Th^+	4065	0.7%	167	0.0%	0	0.0%	0	0.0%
^{232}Th		244	ThC^+	0	0.0%	0	0.0%	0	0.0%	0	0.0%
		248	ThO^+	253355	46.4%	145286	34.1%	15051	6.9%	247	0.3%
		249	$ThOH^+$	143	0.0%	70	0.0%	3	0.0%	0	0.0%
		250	$ThOH_2^+$	450	0.1%	294	0.1%	43	0.0%	0	0.0%
		264	ThO_2^+	257607	47.1%	228716	53.7%	104451	47.8%	22080	29.6%
		265	ThO_2H^+	29778	5.4%	50717	11.9%	98631	45.1%	51968	69.8%
		266	$ThO_2H_2^+$	1081	0.2%	874	0.2%	450	0.2%	180	0.2%
		total cps		546480		426124		218630		74475	
1 ppt	237	237	Np^+	7	1.1%	0	0.0%	0	0.0%	0	0.0%
^{237}Np		249	NpC^+	0	0.0%	0	0.0%	0	0.0%	0	0.0%
		253	NpO^+	33	5.4%	0	0.0%	0	0.0%	0	0.0%
		254	$NpOH^+$	0	0.0%	0	0.0%	0	0.0%	0	0.0%
		255	$NpOH_2^+$	0	0.0%	0	0.0%	0	0.0%	0	0.0%
		269	NpO_2^+	551	89.7%	497	96.1%	310	93.9%	153	90.2%
		270	NpO_2H^+	20	3.3%	13	2.6%	17	5.0%	17	9.8%
		271	$NpO_2H_2^+$	3	0.5%	7	1.3%	3	1.0%	0	0.0%
		total cps		614		517		330		170	
1 ppb	238	238	U^+	7233	1.1%	430	0.1%	0	0.0%	0	0.0%
^{238}U		250	UC^+	0	0.0%	0	0.0%	0	0.0%	0	0.0%
		254	UO^+	26400	4.0%	3421	0.6%	30	0.0%	7	0.0%
		255	UOH^+	10	0.0%	0	0.0%	0	0.0%	0	0.0%
		256	UOH_2^+	50	0.0%	13	0.0%	0	0.0%	0	0.0%

		270	UO_2^+	628191	94.5%	526121	98.8%	356178	99.5%	164464	99.6%
		271	UO_2H^+	464	0.1%	380	0.1%	284	0.1%	127	0.1%
		272	$UO_2H_2^+$	2643	0.4%	1932	0.4%	1371	0.4%	607	0.4%
		total cps		664990		532298		357863		165205	
1 ppt ^{242}Pu	242	242	Pu^+	23	2.9%	0	0.0%	0	0.0%	0	0.0%
		254	PuC^+	0	0.0%	0	0.0%	0	0.0%	0	0.0%
		258	PuO^+	150	18.4%	43	7.4%	0	0.0%	0	0.0%
		259	$PuOH^+$	0	0.0%	0	0.0%	0	0.0%	0	0.0%
		260	$PuOH_2^+$	0	0.0%	0	0.0%	0	0.0%	0	0.0%
		274	PuO_2^+	641	78.7%	544	92.6%	367	100.0%	217	100.0%
		275	PuO_2H^+	0	0.0%	0	0.0%	0	0.0%	0	0.0%
		total cps		814		587		367		217	
1 ppt ^{243}Am	243	243	Am^+	83	9.5%	20	2.8%	2	0.3%	0	0.0%
		255	AmC^+	0	0.0%	0	0.0%	0	0.0%	0	0.0%
		259	AmO^+	788	90.1%	690	96.3%	570	98.6%	298	96.8%
		260	$AmOH^+$	0	0.0%	0	0.0%	0	0.0%	3	1.1%
		261	$AmOH_2^+$	3	0.4%	0	0.0%	0	0.0%	0	0.0%
		275	AmO_2^+	0	0.0%	7	0.9%	7	1.2%	7	2.2%
		total cps		875		716		578		308	
1 ppt ^{248}Cm	248	248	Cm^+	43	7.1%	12	2.7%	0	0.0%	0	0.0%
		260	CmC^+	0	0.0%	0	0.0%	0	0.0%	0	0.0%
		264	CmO^+	556	91.5%	421	97.3%	333	99.0%	178	98.2%
		265	$CmOH^+$	5	0.8%	0	0.0%	3	1.0%	2	0.9%
		266	$CmOH_2^+$	3	0.5%	0	0.0%	0	0.0%	2	0.9%
		total cps		608		433		337		182	

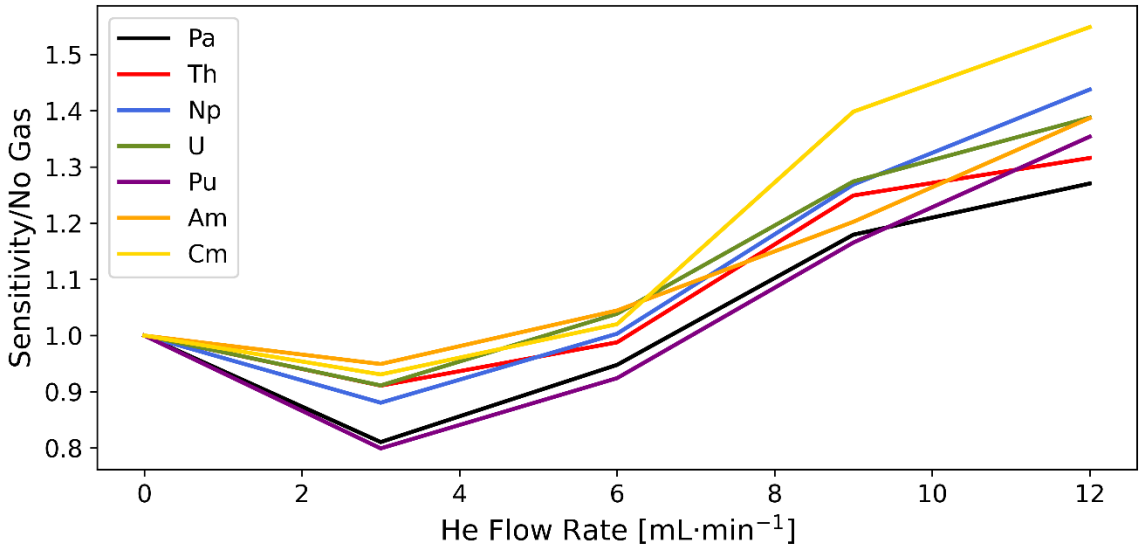

Figure S1: Comparison of measured actinide sensitivity with He gas relative to sensitivity with no gas (cps He mode/cps no gas mode) at various gas flow rates.

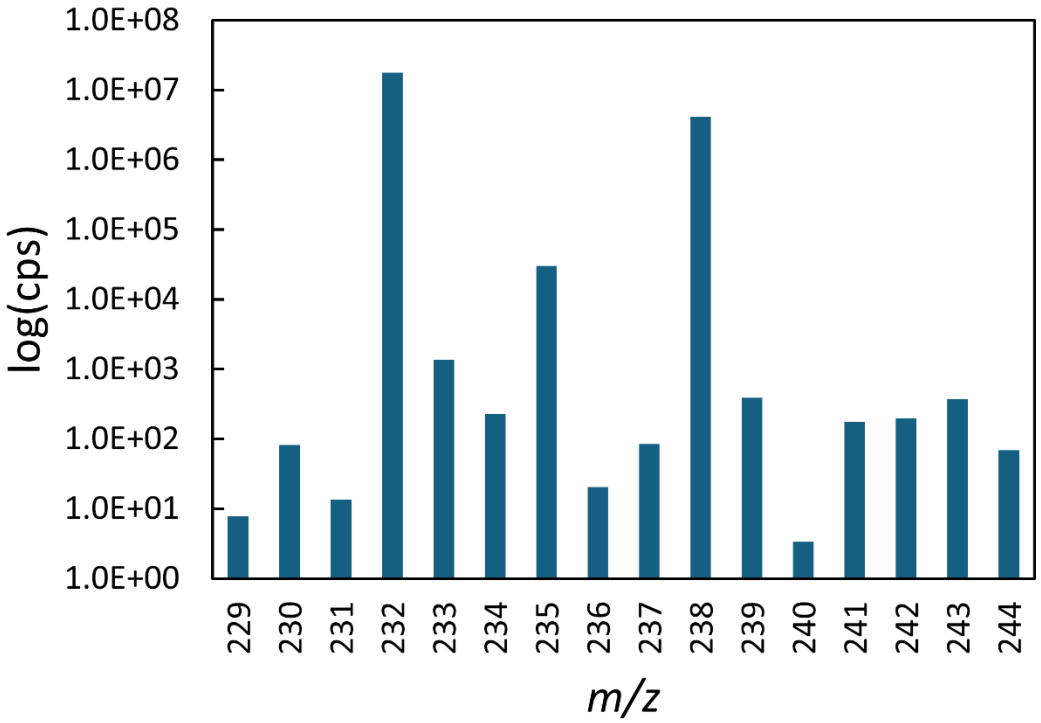

Figure S2: Single quad mass scan (*m/z* 229-244) of a solution containing ~1000 ug·g^{-1} NIST SRM 2711a. While the measured solution contains no ^{241}Am or ^{241}Pu, the on-mass intensity at m/z 241 is ~175 cps, likely related to the high levels of Pb (0.14%) present in NIST SRM 2711a resulting in $^{208}Pb^{16}O_2{}^1H^+$ interferences. Interferences such as this preclude the possibility of accurate analysis of ^{241}Am or ^{241}Pu on mass.

Supporting Text S1. General reactivity of actinide ions (Pa^+, Th^+, Np^+, U^+, Pu^+, Am^+, and Cm^+) with CO_2, O_2, and O_2-He

In general, the actinide ions react with CO_2 to form MO^+ and MO_2^+ species, although appreciable amounts of Am^+ remain unreacted (Fig. 1 main text). Formation of carbide products (MC^+) was not observed with any of the actinides analyzed. In all cases, increasing CO_2 flow rate shifts formation to higher order oxide products, with Pa^+, Th^+, Np^+, and U^+ forming more MO_2^+ and Pu^+, Am^+, and Cm^+ forming more MO^+ product. Both Pu^+ and Np^+ remain predominantly at the MO^+ product; however, ~50% of Pu^+ remains on mass at lower flow rates, whereas ~20% of Np^+ shifts to MO_2^+ at higher flow rates (Fig. 1 main text). While Cm^+ appears to mainly formed MO^+, it is possible Cm^+ reacts to form higher order oxide products (MO_2^+) at higher CO_2 flow rates, but the product ion of $^{248}CmO_2^+$ (*m/z* 280) exceeds the mass range of Q2 on the Agilent 8900. However, in this case, the total ion sensitivity of Cm (sum of all products) is similar to other actinides (e.g., Pu, Np, U; Table S3) and suggests that Cm^+ is not forming MO_2^+. This observation is consistent with data from Matsueda et al. [1], where no CmO_2^+ formation is observed using CO_2 using the NexION 5000 which has a larger mass range. Americium$^+$ was the least reactive with CO_2, with >90% of Am^+ remaining on mass (M^+) at low flow rates (Fig. 1 main text). Using higher CO_2 flow rates does facilitate the formation of AmO^+; however, at the maximum CO_2 flow rate (1.05 mL·min^{-1}) ~60% of Am^+ remains unreacted. At higher CO_2 flow rates, Th^+ formed appreciable amounts (~15%) of the MO_2H^+ species, with all other actinides forming <0.1% MO_2H^+. This product likely resulted from Th^+ reacting with impurities in the reaction gas. [2]

In several cases CO_2 has been used in conjuction with He to facilitate challenging actinide separations, typically targeting U-Pu separations. [3-6] We evaluated the reactivity of actinide ions with 8 mL/min He added to CO_2. The fundamental reactivity of actinide ions is not altered by the addition of He. However, He does help to improve sensitivity, through collisional focusing, with the added benefit of polyatomic interference removal, and thus may still be beneficial when conducting ultra-trace measurements where high flow rates are also necessary.

Actinide reactivity with O_2 and O_2/He gas are shown in Fig. 1 (main text). All reactivity experiments using O_2/He were conducted with the addition of 8 mL·min^{-1} from the dedicated He line on the Agilent 8900. Thus He flow rate (8 mL·min^{-1}) was selected as it yeilded the maximum improvement in sensitivity. Similar to CO_2, the actinides react with O_2 and O_2/He gas to form primarilly MO^+ and MO_2^+ product ions, and higher flow rates shift product ions to higher order oxide products. However, unlike CO_2, the actinides tend to form higher order oxide products (MO_2^+) even

at lower flow rates of O_2 and O_2/He, with <10% of signal remaining unreacted at M^+ for all O_2 and O_2/He flow rates tested (Fig. 1 main text). Specifically, Pa^+, Np^+, U^+, and Pu^+ have a strong affinity to form the MO_2^+ product. However, at low flow rates of pure O_2 (0.225 mL·min^{-1}) significant amounts of MO^+ species are still formed for Pa^+, Th^+, Np^+, U^+, and Pu^+, with the largest amount of MO^+ formed from Th^+ (28%) and Pu^+ (40%) (Fig. 1 main text; Table S3). At higher O_2 flow rates (>0.45 mL·min^{-1}) only Th^+ (6%) and Pu^+ (8%) formed appreciable amounts of MO^+ species and nearly all Pa^+, Th^+, Np^+, U^+ and Pu^+ react to form MO_2^+ ions. At max O_2 flow rates (1.5 mL·min^{-1}) Th^+ and Np^+ form measureable MO_2H^+ product (8% for Th^+ and 3% for Np^+). Americium$^+$ and Cm^+ differ from the other actinides as they predominantly form the MO^+ product with O_2 gas. Even at low O_2 flow rates (0.225 mL·min^{-1}) <5% of Am^+ and Cm^+ remain on mass at M^+, and at higher flow rates the majority of Am^+ and Cm^+ remain at the MO^+ product. However, at the maximum O_2 flow rate (1.5 mL·min^{-1}) a significant amount of Am^+ (~15%) forms MO_2^+ (Table S3). As discussed previously, the Agilent 8900 does not have the ability to detect CmO_2^+; however, as with CO_2 the total ion sensitivity for Cm^+ is similar to other actinide ions (e.g., Pu^+, Np^+, U^+; Table S3), suggesting appreciable CmO_2^+ many not form with O_2 gas. These observations are consistent with data reported elsewhere. [1, 4, 7-10]

Actinide reactivity with O_2/He gas is broadly the same as O_2 gas, although, some differences are noticible. At low flow rates (1.15 mL·min^{-1} O_2/He) a greater fraction (1-10%) of all the actinides remains on mass at M^+ (Table S3). Despite this, Pa^+, Np^+, U^+, and Pu^+ more completely react to MO_2^+ at low flow rates (relative to O_2 alone), with <5% MO^+ product formation for Pa^+, Np^+, and U^+. Thorium is the only actinde to form appreciably more MO^+ product at low flow rates of O_2/He (46.4% vs 28%) relative to O_2 alone. Plutonium also formed appreciable MO^+ product at low O_2/He flow rates, but this is substantially reduced relative to pure O_2 (18.4% vs. 40%). This is likely attributed to the increased number of collisions facilitated by He. The other major difference observed with O_2/He gas is that Am^+ more completely reacts to form MO^+ (i.e. less Am^+ shifts to MO_2^+ even at high gas flows), with <3% of Am^+ shifting to the MO_2^+ product even at maximum O_2/He flow rates (Fig. 1). Finally, while MO^+ and MO_2^+ products are the dominant species formed at high O_2/He flow rates (7.69 mL·min^{-1}), a greater proportion of MOH^+ and MO_2H^+ species are also observed for Am^+ and Cm^+ (up to 1% MOH^+), and Pa^+, Th^+, and Np^+ (up to 69.8% for ThO_2H^+), respectively (Fig. 1).

References

(1) Matsueda, M.; Kawakami, T.; Koarai, K.; Terashima, M.; Fujiwara, K.; Iijima, K.; Furukawa, M.; Takagai, Y. Using CO_2 Reactions to Achieve Mass-spectrometric Discrimination in Simultaneous Plutonium-isotope Speciation with Inductively Coupled Plasma–Tandem Mass Spectrometry. *Chemistry Letters* **2022**, *51* (7), 678-682. DOI: 10.1246/cl.220160.
(2) French, A. D.; Hobbs, K. P.; Cox, R. M.; Arnquist, I. J. The impact of gas purity on observed reactivity with NO using inductively coupled plasma tandem mass spectrometry. *Analyst* **2024**, *149* (24), 5812-5820. DOI: 10.1039/d4an01227e.
(3) Hou, X.; Zhang, W.; Wang, Y. Determination of Femtogram-Level Plutonium Isotopes in Environmental and Forensic Samples with High-Level Uranium Using Chemical Separation and ICP-MS/MS Measurement. *Anal Chem* **2019**, *91* (18), 11553-11561. DOI: 10.1021/acs.analchem.9b01347.
(4) Zhang, W.; Lin, J.; Fang, S.; Li, C.; Yi, X.; Hou, X.; Chen, N.; Zhang, H.; Xu, Y.; Dang, H.; et al. Determination of ultra-trace level plutonium isotopes in soil samples by triple-quadrupole inductively coupled plasma-mass spectrometry with mass-shift mode combined with UTEVA chromatographic separation. *Talanta* **2021**, *234*, 122652. DOI: 10.1016/j.talanta.2021.122652.
(5) Peng, C.; Sun, J.; Zhang, F.; Xing, S.; Liu, X.; Chen, C.; Hou, X.; Shi, K.; Wu, W. Simultaneous Determination of Transuranium Radionuclides in Urine by Tandem Quadrupole ICP-MS/MS with Mass-Shift Mode Combined with Chemical Separation. *Anal Chem* **2024**, *96* (6), 2514-2523. DOI: 10.1021/acs.analchem.3c04699.
(6) Ni, Y.; Bu, W.; Xiong, K.; Hu, S.; Yang, C.; Cao, L. A novel strategy for Pu determination in water samples by automated separation in combination with direct ICP-MS/MS measurement. *Talanta* **2023**, *262*, 124710. DOI: 10.1016/j.talanta.2023.124710.
(7) Kazama, H.; Konashi, K.; Suzuki, T.; Koyama, S.-i.; Maeda, K.; Sekio, Y.; Onishi, T.; Abe, C.; Shikamori, Y.; Nagai, Y. Reaction of Np, Am, and Cm ions with CO_2 and O_2 in a reaction cell in triple quadrupole inductively coupled plasma mass spectrometry. *Journal of Analytical Atomic Spectrometry* **2023**, *38* (8), 1676-1681. DOI: 10.1039/d3ja00136a.
(8) Jaegler, H.; Gourgiotis, A. A new milestone for ultra-low $^{236}U/^{238}U$ isotope ratio measurements by ICP-MS/MS. *Journal of Analytical Atomic Spectrometry* **2023**, *38* (10), 1914-1919. DOI: 10.1039/d3ja00175j.
(9) Jaegler, H.; Gourgiotis, A.; Steier, P.; Golser, R.; Diez, O.; Cazala, C. Pushing Limits of ICP-MS/MS for the Determination of Ultralow $^{236}U/^{238}U$ Isotope Ratios. *Anal Chem* **2020**, *92* (11), 7869-7876. DOI: 10.1021/acs.analchem.0c01121.
(10) Suzuki, T.; Yamamura, T.; Abe, C.; Konashi, K.; Shikamori, Y. Actinide molecular ion formation in collision/reaction cell of triple quadrupole ICP-MS/MS and its application to quantitative actinide analysis. *Journal of Radioanalytical and Nuclear Chemistry* **2018**, *318* (1), 221-225. DOI: 10.1007/s10967-018-6095-7.